Modeling moisture buffering of innovative plasters from material properties to room scale

Journal of Building Engineering 118 (2026) 114983

Contents lists available at ScienceDirect

Journal of Building Engineering

journal homepage: www.elsevier.com/locate/jobe

Modeling moisture buffering of innovative plasters from material properties to room scale

V. Gentile [a,*], G. Autretto [a], M. Libralato [b], S. Fantucci [a], V. Serra [a]

[a] TEBE Research Group, Department of Energy (DENERG), Politecnico di Torino, 10129, Turin, Italy
[b] Polytechnic Department of Engineering and Architecture (DPIA), Università degli Studi di Udine, 33100, Udine, Italy

A B S T R A C T

Passive moisture buffering can stabilize indoor microclimates and reduce cooling energy use, yet reliable prediction across scales remains challenging. This study presents a simplified characterization-to-modeling workflow that links laboratory measurements to room-scale performance. Step-response tests in a dynamic vapour sorption (DVS) analyzer were interpreted with a Fickian diffusion model fitted via root-mean-square error minimization, yielding effective moisture diffusivities of D ~1.84 × 10^{-8} m^2s^{-1} for the lime plaster and D ~1.17 × 10^{-9} m^2s^{-1} for a plaster containing 20 % calcium alginate beads. Vapour-resistance factor functions derived from these fits and from sorption isotherms were validated against NORDTEST MBV dynamic measurements, with the best agreement for both mass change (Δm) and MBV at a surface resistance of 0.1 m^2KW^{-1} (errors: 0.67 % lime; 1.59 % alginate). Year-long building simulations then quantified room-scale impacts: the alginate-enhanced plaster attenuated indoor RH fluctuations more effectively than lime, with attenuation factors spanning from 0.2 to 0.8 depending on the moment of the year and the simulated scenario. Energy analyses showed substantial reductions in latent cooling (up to ~100 % in scenarios with wider indoor relative humidity control band) and up to 11.2 % lower total cooling energy versus lime, with similar sensible loads. The results demonstrate a practical, scalable pathway from material properties to performance, and highlight alginate-enhanced plasters as promising passive components for humidity stabilization and energy-efficient building design and retrofits.

1. Introduction

Hygroscopic building materials interact with ambient air humidity, increasing their water content under humid conditions and reducing it when the air is dry. When the materials can adsorb high moisture contents at ideal environmental conditions, they can passively dampen the effect of high moisture loads in indoor environments (moisture buffering effect). The exploitation of their moisture buffering capacity for the passive control of indoor relative humidity (φ) is of broad interest in contexts such as indoor air quality [1–5], mold prevention [6], the safeguard of structures [7], and the conservation of historical artifacts [8–11], where extreme humidity fluctuations can determine building pathologies.

Considerable effort has been devoted to identifying highly hygroscopic building materials capable of regulating indoor air humidity for the aforementioned applications. Promising results have been found for bio-based and earth-based materials [12–18] and materials admixed or coated with sorbents [19,20].

Unfired and lime-stabilised clay composites have demonstrated strong hygroscopic behaviour and the ability to moderate indoor RH fluctuations, with full-scale simulations in Mediterranean climates confirming reductions in humidification/dehumidification energy by up to 20–30 % when such materials are used as interior finishes [21].

Hemp–lime plasters have been shown exhibiting good Moisture Buffer Value (MBV) ranging from 1.23 to 1.64 g/(m^2.%RH)

* Corresponding author.
E-mail address: vincenzo.gentile@polito.it (V. Gentile).

https://doi.org/10.1016/j.jobe.2025.114983
Received 7 October 2025; Received in revised form 18 November 2025; Accepted 14 December 2025
Available online 23 December 2025

according to the NORDTEST classification highlighting the role of hemp on overall hygrothermal performances [22].

Another study has extended moisture-buffering characterization to cellulose-based material, quantifying a excellent practical MBV around 3 g/(m^2·%RH) and exploring the influence of layer thickness, vapour resistance factor μ, and surface exchange conditions through coupled experimental–numerical analyses [23].

Building on this material-scale understanding, recent modelling work has investigated moisture-buffering plasters at room and building scale: comparisons between NORDTEST tests and single-zone simulations have clarified how ventilation rates, wall build-up, and moisture transport through the envelope modify the effective buffering potential of clay, gypsum, and lime plasters in practice, yielding indoor RH reductions of up to 13 % relative to non-hygroscopic finishes [24]. In addition, extensive review is found in literature [25]. Among these sorbents, Calcium Alginate, the bio-based polymer used in this work, has one of the highest results in terms of MBV [25].Moisture transport in porous building materials is predominantly diffusive and strongly affected by ambient φ fluctuations. This demands accurate knowledge of material properties to realistically reproduce moisture-material interactions under real environmental conditions. Key properties for hygrothermal modelling typically include dry density, porosity, vapour transport coefficient for vapour diffusion, liquid transport coefficient for capillary transport (both drying and wetting), vapour resistance factor, sorption isotherms [26] for moisture retention, thermal conductivity, and heat capacity.

In addition to these fundamental parameters, simplified indicators are often used to describe the overall moisture-buffering behaviour of building materials under cyclic humidity loads. Among them, the MBV and the penetration depth (δ) are the most widely adopted. According to the NORDTEST protocol [27], the practical moisture buffer value ($MBV_{practical}$) quantifies the amount of water exchanged by a material per unit exposed area and per unit change in relative humidity during a daily humidity cycle. It is defined as:

$$MBV_{practical} = \frac{\Delta m}{A \cdot \Delta \varphi} \tag{1}$$

where Δm is the mass of water adsorbed or desorbed over one 24 h cycle, A is the exposed surface area (m^2), and Δφ is the imposed RH step between the high and low levels (%RH). The resulting unit is g/(m^2·%RH), and the value can be classified according to the NORDTEST categories from limited (<0.5 g/(m^2·%RH)) to excellent (>2 g/(m^2·%RH)) buffering performance.

The penetration depth (δ) represents the characteristic thickness within which moisture can penetrate inside a material for given variations in moisture content in a defined time frame, typically set at 24 h to represent daily fluctuations in buildings [27].

With a full hygrothermal characterization and an extensive knowledge of the environmental conditions it is possible to perform detailed numerical simulations considering effects of ventilation, interaction with other wall components, and additional factors not accounted for in laboratory tests. These simulations can be performed with commercially available software based on coupled heat and moisture transfer models originally developed to perform one dimensional moisture related damage risk analyses on single walls (e.g. WUFI® Pro [2,14,28–37], Delphin [38]). Some of these models were then included in whole building modeling tools, enabling to perform dynamic simulations of the interactions between the walls and air.

Some of the software tools are WUFI® Plus [2,14,28–37], TRNSYS [1,3,39], EnergyPlus (using the HAMT – Heat Air Moisture Transfer wall model). These tools allow to compare different wall build ups in different scenarios, making it possible to estimate the moisture content and temperature of the materials, of the air in every thermal zone, and consequently the minimum material layer thickness necessary to obtain a sufficient moisture buffering effect [30,31,40–42]. Moreover, it is possible to estimate thermal energy demands of the zones, identifying potential energy savings.

The two main limitations of these methods are the lack of a comprehensive and reliable dataset of moisture buffering properties for both historical and commercial materials—since available databases often rely on interpolated or simplified values—and the time required to set up and perform the simulations.

Several standardized methods (summarized in Table 1, while detailed information is reported in supplementary material A1) exist to characterize the hygrothermal behaviour of building materials, providing essential input data for simulations or indication on the expected performance. Gravimetric tests (ISO 12570 [43], ASTM C1498 [44]) and sorption isotherm measurements (ISO 12571 [45]) yield equilibrium properties but fail to capture dynamic moisture exchange. Vapour transmission tests (ISO 12572 [46]) provide information on permeability, yet often assume constant values across the *moisture content* range. Dynamic methods such as the NORDTEST protocol [27] are more representative, as they evaluate the moisture buffering value under cyclic humidity variations and could be used to select materials without simulations. ASTM E3054/E3054M [47] further emphasizes the importance of complete and

Table 1
Standards focused on measuring hygrothermal properties under static or dynamic testing conditions.

Reference Number	Name	Scale
ISO 12570 [48]	Hygrothermal performance of building materials and products Determination of moisture content by drying at elevated temperature	Material
ISO 12571:2021 [45]	Hygrothermal performance of building materials and products Determination of hygroscopic sorption properties	Material
ISO 12572:2016 [46]	Hygrothermal performance of building materials and products Determination of water vapour transmission properties — Cup method	Material
NORDTEST [27]	Moisture Buffering of Building Materials	Material/ component
ASTM E3054/E3054M–23 [47]	Characterization and Use of Hygrothermal Models for Moisture Control Design in Building Envelopes	Building simulations

consistent property documentation for hygrothermal modelling. While these standards offer valuable frameworks, they do not fully address the *moisture content* dependent nature of vapour diffusivity.

Permeability, for example, is often treated as a constant [42,49–54]. While this simplification introduces limited errors for conventional cement or lime-based materials (because the affinity with moisture is weak) it becomes problematic for highly hygroscopic materials. By definition, permeability is inherently linked to diffusivity in Fickian transport, which depends on the material's moisture content (C). Moisture diffusivity (D) may exhibit either linear ($D(C) = a_0 + a_1.C$) or exponential ($D(C) = D_0 e^{-\beta C}$) dependence on water content [55,56].

In this study, a methodology is proposed to derive the vapour diffusivity coefficient from the profile of the dynamic moisture uptake measurements used for the vapour sorption isotherm, obtained at constant temperature and stepwise φ variations. This modelling framework builds upon experimental data previously obtained for the same samples in Gentile et al. [25], ensuring continuity between laboratory characterization and model-based validation. By combining diffusive transport modelling and sorption equilibrium isotherm, the vapour resistance factor (μ) is evaluated as a function of equilibrium φ (and therefore of the equilibrium moisture content). The resulting properties are used as input for material-level dynamic simulations using the coupled heat and moisture transfer tool WUFI® Pro, to validate the model comparing the dynamic moisture uptake measured during the moisture buffering test procedurefollowing the NORDTEST protocol.

This approach is applied to a newly developed hygroscopic plaster made by combining alginate-based aggregates with conventional lime plaster, and to a reference lime plaster used as baseline. The validated material properties are then implemented into room scale simulations defined WUFI® Plus to evaluate the material's ability to passively regulate indoor humidity under realistic boundary conditions. The simulations of an office room with alginate plaster interior finishing are carried out and compared with those using conventional lime plaster, with a focus on humidity regulation performance, potential energy-saving for indoor climate control [4, 54–56] and impact on occupants' thermal comfort [4,57].

Although several studies have investigated the hygrothermal behavior of bio-based and mineral plasters [4,57–59], few have provided a unified workflow that connects experimental sorption characterisation, parameter derivation, and validation across multiples scales. In particular, the propagation of experimentally derivated hygroscopic parameters – such as μ(φ) – into dynamic building simulations remain limited, often relying on assumed or constant values that overlook their dependence on relative humidity.

The present work addresses this gap by proposing and validating a multiscale framework that links laboratory characterisation, model calibration, and room-scale performance analysis. Specifically, the study aims to:

(i) establish a consistent procedure for deriving and validating μ(φ) function from DVS and NORDTEST data;
(ii) verify the ability of the derived parameters to reproduce experimentally observed moisture buffering behaviour;
(iii) quantify the impact of alginate-based plaster on indoor RH stability and cooling energy demand relative to conventional lime plaster.

2. Methodology

In this study, we formulate a methodology to estimate material properties from the experimental data to correctly model an innovative plaster based on composite lime/alginate at the room scale. Following the experimental investigation presented in Gentile et al. [25], where the plaster formulations were formulated and characterized, the present work applies a numerical modelling framework to assess the hygrothermal performance of an innovative plaster compared to a conventional one.

The materials under analysis are two of the plasters previously developed [25] Specifically, two of them have been selected: (i) a reference lime-based mortar, hereafter referred to as *lime plaster*, and (ii) a plaster with 20 wt% calcium alginate beads, previously labelled as B02, hereafter referred to as *alginate plaster*.

In section 2.1 we explain how to derive diffusivity coefficients from the first experimental dataset (DATASET-1). DATASET-1contains the adsorption isotherms of the two considered plasters obtained using the DVS Analyzer proUmid Vsorp Basic, during the experimental campaign reported in Gentile et al. [50]. These data, previously presented and discussed in that work, provide the basis for the present diffusion analysis. [25]. Isotherms are obtained with a 10 % step variation on φ, from 40 % to 70 %, at constant 23 °C, both in sorption and desorption. By fitting numerical models with DATASET-1 (section 2.1.2), we defined a plaster diffusivity coefficient as a function of air φ. The material-level modelling progresses by validating this diffusivity function, comparing numerical data with DATASET-2. The DATASET-2 [25] contains experimental results from moisture buffering tests operated according to the NORDTEST protocol on the same materials, obtained during the experimental campaign reported in Ref. [50]. Finally, it ends by transferring estimated material data into simulation models at the material scale using the WUFI® Pro software. Specifically, in section 2.1.4, we outline the derivation of a vapour resistance factor function based on the diffusivity function discussed in section 2.1. We then validate the two materials property sets implemented in WUFI® Pro, comparing the simulated mass variation and MBV of the samples with the ones measured. Subsequently, we conduct simulations at the room level using WUFI® Plus to assess the impact of alginate plaster adoption on indoor φ, comparing it against the reference one, lime plaster, using an established index. In addition to the hygrothermal performance comparison, we also evaluated the consequent energy saving for room cooling and dehumidification due to the application of the *alginate plaster*.

2.1. Modelling at the material scale

2.1.1. Diffusive model for moisture transport at material scale

Moisture diffusion in porous building materials is classically modelled through Fick's second law, which, under the assumption of constant diffusivity and equilibrium moisture content, admits an analytical solution (supplementary material section A2). However, under realistic conditions where moisture content and environmental conditions vary over time, the diffusivity $D(C)$ becomes a function of moisture content of the hygroscopic material. Therefore, a time-dependent, nonlinear diffusion model must be solved numerically.

$$\begin{cases} \dfrac{\partial C(x,t)}{\partial t} = \dfrac{\partial}{\partial x}\left[D \cdot \dfrac{\partial C(x,t)}{\partial x}\right] \\ \left.\dfrac{\partial C(x,t)}{\partial x}\right|_{x=0,t} = 0 \\ C(x=+L,t) = C_{eq}(t) \\ C(x,t=0) = C_0 \end{cases} \tag{2}$$

The governing Eq. (2) in one dimension is discretized in space using a central finite difference scheme and in time using a fully implicit (backward Euler) method. The spatial domain is divided into N_x+2 nodes (including boundaries), and the temporal domain into N_t+2 timesteps. The resulting system of nonlinear algebraic equations is solved iteratively, each time step, with the boundary conditions reported in system (2). The Neumann condition with zero flux at the bottom boundary ($x = 0$) reflects the experimental condition in which the sample's bottom surface is sealed (e.g., with aluminum tape in our experiment), blocking any moisture exchange [25]. On the contrary, at the top boundary $(x=N_x+1=+L)$ a Dirichlet time-dependent condition imposes an equilibrium concentration, $C_{eq}(t)$, corresponding to the imposed φ step. The function $C_{eq}(t)$ is determined from gravimetric equilibrium mass under known φ conditions and remains piecewise constant over each φ step (e.g., 40 %, 50 %, 60 %, etc.). The initial condition reflects the mass of the sample at the end of the preconditioning. For example, when using data coming from the NORDTEST testing protocol the initial condition is 50 %. On the contrary, when using data from the equilibrium isotherm, the previous step equilibrium φ is used.

2.1.2. Fitting procedure and validation of diffusivity

To solve the nonlinear system in Eq. (1), at each time step, an implicit iterative method is employed. Specifically, the system of nonlinear equations resulting from the discretization is solved using a root-finding algorithm, where we define a residual function $F(C_t+1)$ expressing the deviation from mass balance for each node. The iterative procedure is based on the Newton-like method, which requires solving Eq. (2) for the unknow vector reported in Eq. (3).

$$F\left(C^{t+1}\right) = 0 \tag{3}$$

$$C^{t+1} = \left[C_0^{t+1}, C_1^{t+1}, \ldots, C_{N_x+1}^{t+1}\right] \tag{4}$$

Given the nonlinearity introduced by $D(C)$, the Jacobian matrix is not computed explicitly. Instead, the modified Powell's hybrid method is used, that combines the robustness of the Newton method with global convergence properties of trust-region strategies [60]. This approach ensures stability of the numerical solution, especially under steep φ gradients, while avoiding divergence in the presence of strong nonlinearity in $D(C)$. The system in Eq. (2) is then discretized and numerically solved with Eq. (5).

$$\begin{cases} F_j = C_j^{t+1} - C_j^{t} - \Delta t\left[\dfrac{\left.\frac{\partial D(C)}{\partial C}\right|_{C_j^{t+1}}\left(C_{j+1}^{t+1\,2} - 2C_{j-1}^{t+1}C_{j+1}^{t+1} + C_{j-1}^{t+1\,2}\right)}{4h^2} + \dfrac{D\left(C_j^{t+1}\right)\left(C_{j+1}^{t+1} - 2C_j^{t+1} + C_{j-1}^{t+1}\right)}{h^2}\right] \\ F_0 = C_0^{t+1} - C_1^{t+1} \\ F_{N_x+1} = C_{N_x+1}^{t+1} - C_{eq}\left(t^{t+1}\right) \end{cases} \tag{5}$$

Where h is the spatial distance between two adjacent nodes and corresponding to $h = L/(N_x+1)$. In this study we used a functional form of Eq. (6) for $D(C)$, that has been proved in previous study on alginate-based polymers useful for the description of moisture mass exchange [55,56].

$$D(C) = a_0 + a_1 C \tag{6}$$

The parameters a_0 and a_1 are estimated by minimizing the total squared deviation, reported in Eq. (7), between simulated, $C(x, t_i; a_0, a_1)$, and experimental domain-averaged concentrations, $C_{\exp}(t_i)$:

$$err(a_0;a_1) = \sum_{i=1}^{N_{exp}}\left[\frac{1}{L}\int_0^L C(x,t_i;a_0,a_1)dx - C_{exp}(t_i)\right]^2 \tag{7}$$

The fitting procedure was applied to DATASET-1 to derive the function of the diffusivity coefficient $D(C)$ per sample.

2.1.3. Calculation of the vapour resistance factor

In commercial software tools for the building envelope simulation, the material permeability to water vapour is described by the μ factor, the water vapour resistance factor, derived from the material water vapour permeability. In principle, the calculation of permeability requires the knowledge of the diffusivity (D) and the solubility (S) [61]. When analyzing water vapour transport in porous solids (as a building material can be exemplified), the solubility corresponds to the moisture capacity defined from the derivative of material moisture content (expressed as kg/m^3). Moisture capacity is expressed in kg/(m^3 Pa). The permeability δ_p is defined and the vapour resistance factor are defined as:

$$\delta_p = S \cdot D = \frac{\partial C}{\partial p} D \tag{9}$$

$$\mu(p) = \frac{\delta_{p_{air}}}{\delta_{p_{moisture}}} = \frac{D_{air}}{D_{H2O}(p) \cdot \frac{\partial C(p)}{\partial p}} \tag{10}$$

In a variable regime, moisture content C and diffusivity coefficient D vary with temperature and humidity. Hence, the moisture permeability is a function of T and φ (or p) rather than a constant number. As function of T and φ (or p), the solubility is obtained by interpolating sorption isotherms with a 3rd degree polynomial equation with a fixed point at 0 kg/m^3 for 0 Pa (Eq. (11)).

$$C(p) = a \cdot p^3 + b \cdot p^2 + c \cdot p \tag{11}$$

The materials data used for the polynomial interpolation of the isotherm and of the $\mu(\varphi)$ are reported in supplementary material A4. In this study, we used only one isotherm at 23 °C, as the applications of the materials are at room temperature between 20 °C and 25 °C. This aspect also represents a main limitation of available simulation tools, because they accept only one isotherm (usually at 23 °C) instead of a family of curves.

2.1.4. Validation of moisture buffer behaviour on WUFI® Pro

Based on the previously derived $\mu(\varphi)$ and other geometric and thermophysical specifications reported in Table 2, the two samples have been modelled in WUFI® Pro, a one-dimension transient heat and moisture calculation software which is able to determine the hygrothermal performances of building components under real climate conditions. The objective is to replicate the NORDTEST protocol conditions within the software to validate the materials by comparing the measured data of mass variation during the cycles with the simulated results. Upon successful validation, the materials were implemented in WUFI® Plus to simulate a case study of an indoor environment and assess their ability to passively control indoor relative humidity fluctuations, as well as their impact on the room's energy consumption.

The first step in the simulation process involved selecting *Cement Plaster* ("*stucco*", A-value: 0.51 kg/m^{2}h$^{0.5}$) from the Fraunhofer-IBP Mortar and Plaster folder of the WUFI database as the reference material. The A-value represents the water absorption coefficient according to EN ISO 15148, originally defined in kg/(m^2·s$^{0.5}$) [5]) and expressed in hours in the WUFI® database for consistency with the software's time unit. Starting from this dataset, the experimentally measured properties were modified and while the permeability is the one obtained from the diffusivity optimization analysis described in the previous sections. The complete set of adopted properties is reported in Table 3.

The surface heat transfer coefficients for both the inner and outer faces of the samples were carefully defined to represent realistic moisture and heat exchange conditions. In WUFI® Pro, moisture transport is treated analogously to heat transfer, so these coefficients were fine-tuned to simulate various indoor environments, accounting for convective and radiative contributions. Since the lower surface of the samples was sealed with an acrylic silicone coating and aluminum tape to prevent vapour exchange during testing, this condition was reproduced in the model by doubling the sample thickness, thereby ensuring consistency with the experimental setup [25]. The initial conditions in the simulation were aligned with the preconditioning phase of the experimental tests, assuming a relative humidity of 50 % and a temperature of 23 °C. The simulation control parameters, including the calculation period and time step, were set to reflect those adopted during the laboratory tests. The simulation was run in combined heat and moisture transfer mode, enabling the inclusion of all relevant hygrothermal processes to accurately reproduce the dynamic response of the material. External and internal climates were identically set based on the specific climate files, reflecting measured values from the DVS tests used during the NORDTEST protocol [25].

The results of the simulations were thoroughly analysed and compared to the experimental data as follows:

- The measured and simulated values of mass variations Δm and MBV were compared by calculating percentage errors between the two values for each surface resistance and for each material. This approach allowed for a detailed assessment of the simulation's accuracy in predicting the moisture behaviour of the materials under test conditions.
- The trends of measured and simulated mass variations with a surface resistance of 0.1 m^{2}K/W were compared for each material, as detailed in paragraph 3.1.3 and in section A4 of the Supplementary. This comparison helped assess the consistency of the simulation outcomes with the hygrothermal characterization.

Table 2
Summary of inputs, boundary conditions and output for the simulation on WUFI® Pro at the material level, for all the 4 samples.

Input			Boundary and initial conditions		Output	Post-processing	Validation
Geometry	Thermophysical	Hygroscopic	Temperature	Humidity	–	–	–
Material thickness (measured)	Dry density (measured) Porosity (Fraunhofer-IBP WUFI database) Specific Heat Capacity (Fraunhofer-IBP WUFI database) Thermal conductivity (measured) Interior/Exterior surface heat resistance (0.1, 0.13, 0.15, 0.20, 0.22)	Moisture Storage Function (sorption isotherm measured at 23°) Water Vapour Diffusion Resistance factor moisture dependent (extracted from data + fitting)	As in NORDTEST experiments - 7 cycles with 23 °C constant Preconditioning at 23 °C for 15 days	As in NORDTEST experiments - 7 cycles of 24 h (8h $\varphi = 75$ %, 16h $\varphi = 33$ %) Preconditioning at 50 % for 15 days	Material moisture content	Mass variation (Δm) MBV simulated	Percentage error analysis of measured vs. simulated Δm and MBV to assess model accuracy Trends comparison of Δm measured and simulated for validation. Overlay of measured and simulated Δm trends to validate agreement with experimental data. Dispersion analysis of measured vs. simulated Δm to assess model reliability

Table 3
Material properties used as inputs to model the behaviour of the two plasters.

Geometry		Lime plaster	Alginate plaster
Material tickness [m]	(measured x 2) [25]	0.0278	0.0272
Thermophysical			
Dry density [kg/m^3]	(measured) [25]	1761	1611
Porosity [m^3/m^3]	(Fraunhofer-IBP WUFI database)	0.3	0.3
Spec. Heat Capacity [J/kgK]	(Fraunhofer-IBP WUFI database)	850	850
Thermal conductivity [W/mK]	(measured) [25]	0.408	0.632
Hygroscopic			
Water Vapour Diffusion Resistance Factor [−]	(calculated by the value of μ-value vs φ) [section A4 supplementary]	4.76	6.14
Water content [kg/m^3] vs φ [%]	(measured) [25] [section A4 supplementary]	$w(0.40) = 4.52$	$w(0.40) = 57.07$
		$w(0.45) = 4.67$	$w(0.45) = 71.11$
		$w(0.50) = 5.14$	$w(0.50) = 87.14$
		$w(0.55) = 5.70$	$w(0.55) = 99.19$
		$w(0.60) = 5.95$	$w(0.60) = 113.99$
		$w(0.65) = 6.73$	$w(0.65) = 131.70$
		$w(0.70) = 7.30$	$w(0.70) = 149.53$
		$w(0.75) = 7.75$	$w(0.75) = 168.64$

- The differences in mass change Δm measured and simulated with a surface resistance of 0.1 m^{2}K/W were compared for each test cycle and for each material. This analysis, also detailed in the supplementary materials (section A4), was used to evaluate the data dispersion relative to bisector in the measured vs. simulated graphs, providing insights into the accuracy of the simulation model.

This validation step was crucial to ensure that the model reliably represented the material behaviour under varying hygrothermal conditions.

Following the successful validation, the verified material properties and models were transferred to WUFI® Plus for further simulation at the room scale. This included simulating the effects of the validated materials on indoor climate control and energy efficiency in a case study building, providing insights into their practical implications in real-world applications.

2.2. Modelling at room scale

To evaluate the impact of the different plasters on the building cooling and dehumidification demand, the validated material properties of the plasters were used as input data to perform building-level simulations of an office room. The software used is WUFI® Plus, that integrates the heat and moisture transfer wall model of WUFI® Pro in a whole building model [62].

The case study considered is a living-lab, TEBE L^{2}AB, with a floor surface of 10 m^2 with south-west exposure, located in Politecnico di Torino in Turin, Italy (45°04′45″N 7°40′34″E). The real shape of the room is described in Fig. 1.

This space was chosen in particular because it replicates an actual experimental setting created as part of the Horizon 2020

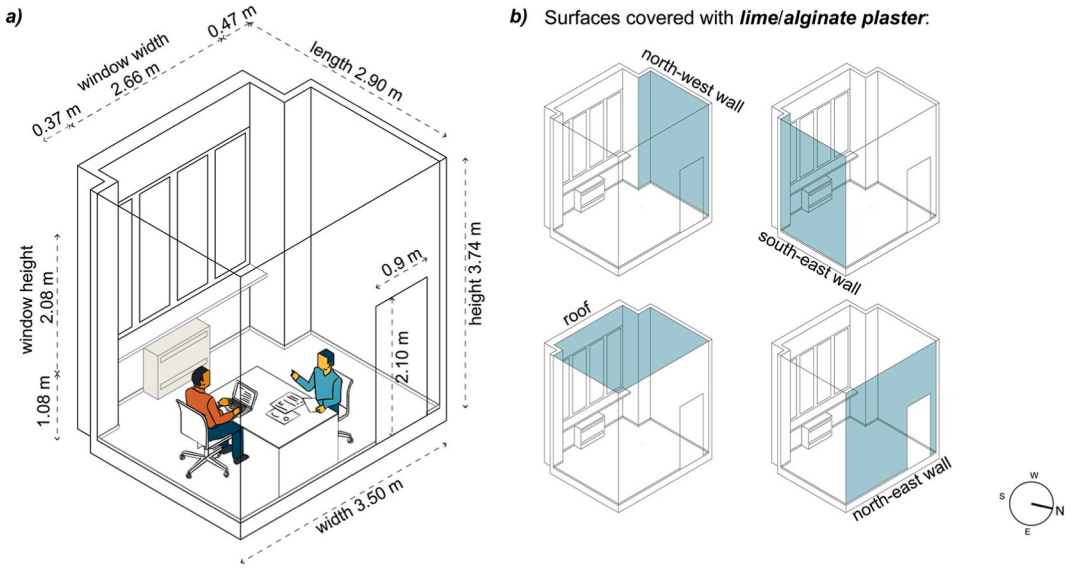

Fig. 1. Case study: a) Axonometric view of the simulated office room, b) Surfaces covered with lime plaster/alginate plaster in different simulation scenarios.

European project "Iclimabuilt" [63]. It is a focal point for ongoing tests and future research on the moisture buffering capacity of highly hygroscopic components in a controlled setting [64].

The lime plaster and the alginate plaster are used alternatively as the internal layers in the multi-layer wall/ceiling assemblies (Table 4) within a standard office room covering an exposed surface of 43 m^2. These simulations are conducted under typical operational conditions that reflect a common office occupancy pattern with two occupants, 5/7 days present.

In the model, all room surfaces (walls, floor, ceiling) except the external wall were modelled with adiabatic boundary conditions, as adjoint to thermal zones with the same internal conditions. Heat and moisture gains due to occupancy were approximated using standard values from the WUFI® Plus database—specifically, 156 W and 162 g/h for two adults performing office/typing work, based on guidelines from ASHRAE 55 [65] and IEA Annex 41 [66]. The infiltration rate was set as 0.50 Air Changes per Hour (ACH) (UNI EN 16798–1:2019 [67]).

For the boundary conditions, the climate file for Turin from the WUFI database was selected to reflect local environmental conditions. Various indoor climate control scenarios were modelled using an ideal HVAC system for heating, cooling, humidification, and dehumidification. These scenarios are detailed in Table 5 under the "Indoor control" section, outlining the comprehensive strategy for the hygrothermal simulation of the office.

To obtain a full year accurate result, independent of the initial conditions, the model simulated five consecutive years. The data for each year was overlapped, and the data from the year that was identical to the previous one, was selected for analysis and post-processing.

Results from the simulations were post-processed and analysed to determine: *i*) Attenuation of relative humidity fluctuations; *ii*) Dehumidification and cooling energy demand.

i) Attenuation of relative humidity fluctuations.

This analysis focused on evaluating the ability of the enhanced alginate plaster to damp internal humidity fluctuations compared to the reference lime plaster. The effectiveness of alginate plaster in stabilizing indoor humidity fluctuations was quantified by the attenuation factor f_φ, calculated as follows Eq. (11):

$$f_\varphi = 1 - \frac{(\varphi_{max} - \varphi_{min})_{\text{alginate plaster}}}{(\varphi_{max} - \varphi_{min})_{\text{lime plaster}}} \tag{11}$$

where φ_{max} and φ_{min} refer to the maximum and minimum recorded daily relative humidity levels for lime plaster and alginate plaster

Table 4
Material properties applied in the numerical modelling of the case study.

Partition/stratigraphy	Vapour diffusion resistance factor [−]	Thermal conductivity [W/mK]	*Specific heat capacity* [J/kgK]	*Density* [kg/m^3]
External wall (R_{si} = 0.13 m^2K/W; R_{se} = 0.04 m^2K/W)				
Solid Brick ARB – 12 cm	10	0.695	861	1807
Air Layer – 12	0.11	0.723	1000	1.3
Aerated Clay Brick – 25 cm	4	0.12	850	672
Interior Plaster (Gypsum Plaster) – 2 cm	8.3	0.2	850	850
Internal wall (R_{si} = 0.13 m^2K/W)				
Interior Plaster (Gypsum Plaster) – 1 cm	8.3	0.2	850	850
Gypsum Board – 1.25 cm	6.8	0.193	732	1384
Mineral Insulation Board – 7 cm	3.4	0.043	850	115
Gypsum Board – 1.25 cm + **lime plaster/alginate plaster (20 %)** – 2 cm	6.8	0.193	732	1384
Floor (R_{si} = 0.17 m^2K/W; R_{se} = 0.04 m^2K/W)				
Granite – 1.5 cm	54	1.66	702	2453
Cement Plaster – 2 cm	25	1.2	850	2000
Concrete Screed, mid layer – 2 cm	69	1.6	850	1970
Brick H – 26 cm	14	0.955	860	1891
Interior Plaster (Gypsum Plaster) – 2 cm	8.3	0.2	850	850
Roof (R_{si} = 0.1 m^2K/W; R_{se} = 0.04 m^2K/W) + **lime plaster/alginate plaster (20 %)** – 2 cm				
Interior plaster (Gypsum plaster) – 2 cm	8.3	0.2	850	850
Brick H – 26 cm	14	0.955	860	1891
Concrete Screed, mid layer – 2 cm	69	1.6	850	1970
Cement Plaster – 2 cm	25	1.2	850	2000
Granite – 1.5 cm	54	1.66	702	2453
Door (R_{si} = 0.13 m^2K/W)				
Eastern White Cedar	16515	0.091	750	360
Window (R_{si} = 0.13 m^2K/W; R_{se} = 0.04 m^2K/W)				
U-value = 1.91 W/m^2K	Frame factor = 0.7	Solar energy transmittance hemispherical (g-value): 0.30		

Table 5
Summary of inputs, boundary condition and output for the simulation on WUFI® Plus at the building level, for only 1 sample.

Input				Output	Post-processing
Material	Building	Indoor control	Outdoor	–	–
• same as in Table 3	• localization (Turin) and orientation (South-West) as the living-lab • wall stratigraphy according to material inputs and living lab • size of opaque and transparent surfaces • occupancy schedule (Mon-Fri, h:8–18) • internal loads (2 adults, office - typing [65,66]) • ventilation due to only infiltration 0.5 1/h [67] • HVAC ideal: several cases of indoor temperature and relative humidity control	Case 1: temperature control between 20 °C and 26 °C during the working hours (8-18) and between 15 °C and 30 °C during the rest of the day (18-8) • Case 1.1: no φ control • Case 1.2: φ control between 40 % and 60 % during the working hours (8-18) and left uncontrolled during the remaining hours (18-8). • Case 1.3: φ control between 30 % and 70 % during the working hours (8-18) and left uncontrolled during the remaining hours (18-8). Case 2: - *heating season* (from 01/01 to 15/04 and from 15/10 to 31/12): temperature set at 20 °C during working hours (8-18), fluctuating between 15 and 30 °C during the rest of the day (18-8); - *cooling season* (from 16/04to 14/10): temperature set at 26 °C C during working hours (8-18), fluctuating between 15 and 30 °C during the rest of the day (18-8). • Case 2.1: no φ control • Case 2.2: φ control between 40 % and 60 % during the working hours (8-18) and left uncontrolled during the remaining hours (18-8). • Case 2.3: φ control between 30 % and 70 % during the working hours (8-18) and left uncontrolled during the remaining hours (18-8).	• Turin from WUFI® Plus database	• *T* Outdoor [°C] • *T* Indoor [°C] • φ Outdoor [%] • φ Indoor [%] • Humidification load [kg/h] • Dehumidification load [kg/h] • Cooling power [kW]	• Attenuation of φ fluctuations: calculation of f_φ (comparison with reference sample) • Dehumidification loads and cooling energy demand: calculation of annual latent and sensible cooling demand (kWh/m^2, kWh/m^3). Assessment of the percentage reduction in energy consumption compared to lime plaster. • Indoor φ cumulative frequencies: % of hours with φ within the comfort interval (comparison with the reference sample)

respectively. The f_φ-factor is a dimensionless index that can assume values lower than or equal to 1. Positive values indicate attenuation of indoor relative humidity fluctuations by the alginate plaster, while negative values would correspond to amplification, i.e., humidity fluctuations in the case with alginate plaster than in the lime plaster one. The f_φ-factor thus quantifies the reduction in the range of relative humidity fluctuations, indicating the enhanced plaster's effectiveness compared to the reference lime plaster. A higher f_φ factor signifies a greater capability of the alginate enhanced plaster to stabilize humidity fluctuations within the environment.

ii) Dehumidification and cooling energy demand.

The impact of alginate plasters on the room's energy demand was evaluated by analyzing both latent and sensible components of the annual cooling demand under selected indoor climate control strategies. The analysis considered all simulated cases (Cases 1.1 to 2.3, as detailed in Table 5). However, dehumidification loads were present only in Cases 1.2, 1.3, 2.2, and 2.3, where relative humidity control was imposed. In contrast, in Cases 1.1 and 2.1, where no φ control was applied, only the sensible cooling demand was considered.

The latent cooling demand was extracted from WUFI® Plus as the dehumidification load, expressed as the amount of water removed from indoor air [kg], and then converted into energy [kWh] using the latent heat of vaporization of water (~2250 kJ/kg at room temperature). The sensible cooling demand [kWh], on the other hand, was directly obtained from WUFI® Plus as the hourly integral of "Cooling Power" [kW], representing the energy required to maintain indoor air temperature within the setpoint range. The total annual cooling demand for each case was calculated by summing the latent and sensible components.

To evaluate the effectiveness of alginate plasters, relative savings in both latent cooling demand and total cooling demand were calculated with respect to the lime plaster configuration within each case. The share of latent over the total cooling was also computed. This evaluation highlights the potential of moisture-buffering plasters to reduce latent loads and overall cooling energy demand, supporting the development of efficient passive strategies for indoor environmental control.

3. Results and discussion

3.1. Fitting diffusivity model with DATASET-1

Fig. 2a and b report the moisture content evolution of the super hygroscopic plaster obtained by mixing a conventional lime plaster with 20 % of alginate beads (hereafter defined as "alginate plaster") during stepwise φ variations, showing adsorption (increase) and desorption (decrease), respectively. The mass measures have different durations as they were measured until the equilibrium is reached with the criterion of mass variations lower than 0.01 % for more than 300 min. Experimental data from DVS are compared with model predictions obtained through Eq. (1) after the iterative optimization described in Section 2.1.2. A good agreement is observed, with the two trends largely overlapping. This is further quantified in Fig. 2c, which presents the distribution of the relative error for each φ step in both the lime plaster (blue) and alginate (green) plasters. In most cases, the median relative error falls within ±2 %, while only a limited number of outliers for the lime plaster extend toward ±5 %. These deviations are attributed to truncation errors at very low moisture contents, since lime plaster exhibits a moisture uptake two orders of magnitude smaller than alginate at the same φ step (as shown in Fig. 4).

Fig. 3 reports the distribution of the coefficients a_0 and a_1 that define the diffusivity function of Eq. (5) for both lime plaster and alginate plasters. Each value obtained from the optimization algorithm of section 2.1.2 required 40–50 iterations for the residual of Eq. (6) to reach the target tolerance of 10^{-7}. Supplementary materials in sections A3 and A4 provide a picture of the good accuracy the diffusion model, having fitting errors for each humidity step within ±1 % of the gravimetric measurements of the DVS. The algorithm required no more than 20 s to process 100 h of data. For both materials, the coefficient a_1 is several orders of magnitude smaller than a_0, implying that the diffusivity coefficient in the φ range of 0–70 % can be considered almost constant and approximated by a_0. The geometric mean of D reveals a marked difference between the two plasters, with lime plaster showing $D \sim 1.84 \times 10^{-8}$ $m^2 s^{-1}$ and alginate $D \sim 1.17 \times 10^{-9}$ $m^2 s^{-1}$. Moisture transport in porous materials governed by Fick's law has a characteristic penetration depth $\ell = \sqrt{Dt}$ defined over a transient of duration t[61]. Under cyclic boundary conditions with period T, the effective penetration depth is

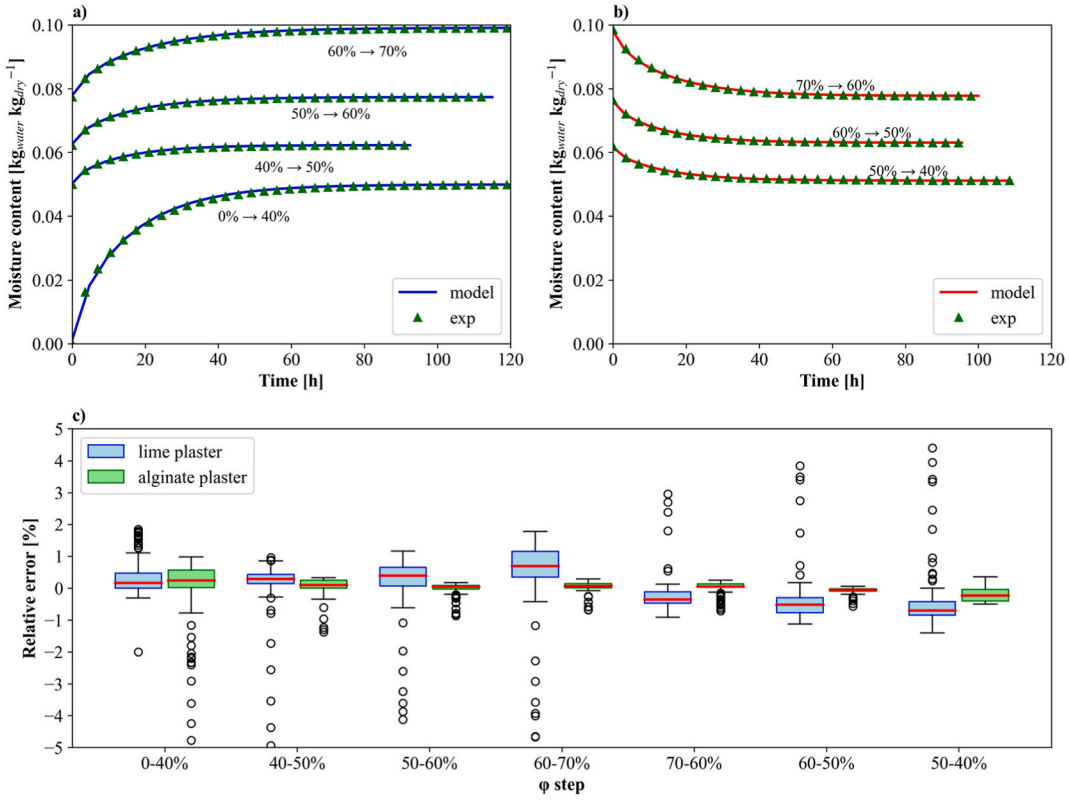

Fig. 2. Results of diffusion model algorithm fitting different tests on samples with alginate plasters. In a) the adsorption stage, while in b) the desorption stage. In c) the distribution of the relative error at each humidity step is reported for both the lime plaster and the alginate plasters.

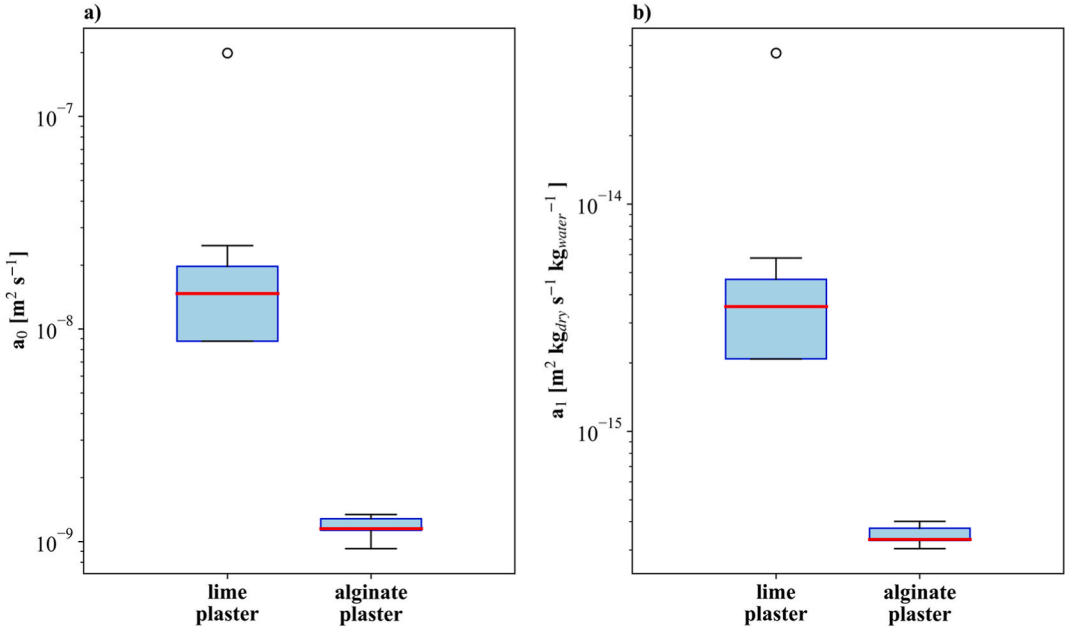

Fig. 3. In a) the distribution of the values of coefficient a_0 coming from the optimization algorithm for the lime plaster and the alginate based plaster. In b) the distribution of the same values for the coefficient a_1.

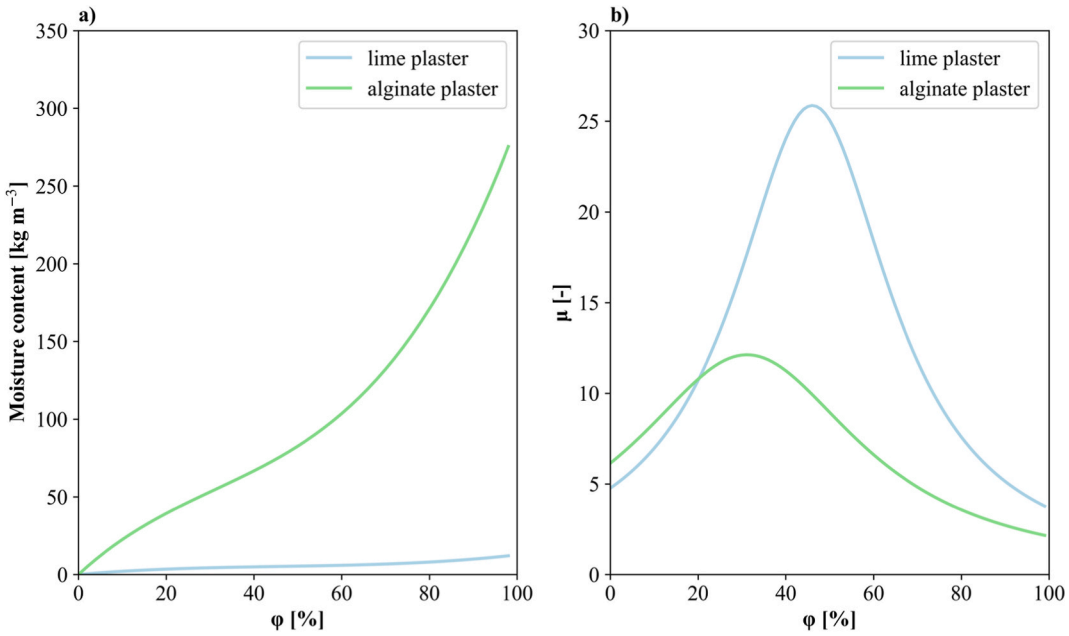

Fig. 4. In a) the sorption isotherms of lime plaster and alginate plasters. In b) the vapour resistance factor μ derived from Eq. (9).

instead given by $\delta = \sqrt{DT/\pi}$ [27,68,69], which corresponds to the thickness of material actively involved in moisture exchange during one cycle. Application of these relations shows that, for an 8 h step, moisture penetrates approximately 22.5 mm into lime plaster compared to only 5.7 mm into alginate, while for daily cycles (24 h) the penetration depths are 13.0 mm and 3.3 mm, respectively. This indicates that only the first few millimeters of alginate plaster contribute significantly to buffering during sub-daily cycles, whereas lime plaster engages a substantially thicker layer. Nevertheless, despite its relative slower kinetics, alginate exhibits a sorption capacity nearly two orders of magnitude higher than lime plaster at comparable RH steps (see Fig. 4). As a result, even relatively thin layers of alginate can outperform lime plaster in terms of absolute buffering potential under realistic indoor humidity fluctuations.

3.2. Extrapolation of vapour resistance functions

The application of Eq. (9) to the sorption isotherms reported in Fig. 4a leads to the vapour resistance factor curves shown in Fig. 4b, highlighting their dependence on relative humidity. The alginate plaster exhibits consistently lower values of μ within the φ range 30–70 %, with a peak shifted towards lower humidity (~30 %), whereas the lime plaster reaches its maximum around 50 % φ. The shape of the two curves is mathematically defined by the moisture capacity obtained by the fitted functions of the sorption isotherms and might not reflect the μ values in the extrapolation relative humidity ranges. The narrower range of μ for alginate indicates a more stable vapour transport resistance across the hygroscopic interval, while the lime plaster shows a sharper peak and thus a stronger sensitivity to φ variations. This behaviour reflects the higher sorption capacity of alginate, which reduces the effective resistance to vapour flow, whereas lime plaster, with lower water uptake, translates small variations in sorption into pronounced changes in μ. From a practical perspective, this implies that alginate plaster ensures more uniform hygric behaviour under fluctuating indoor humidity, whereas lime plaster may hinder vapour transport particularly around mid-range φ values.

Representing the moisture sorption curve with Eq. (10), the curves of the two plasters could be described using the parameters presented in Table 6, obtained from a least square interpolation.

These values are then used to obtain the vapour resistance factor as a function of relative humidity, using equation (12):

$$\mu(\varphi) = \frac{D_{air}}{D_{H2O} \cdot \left(3a \cdot \varphi^2 \cdot p_{sat}^2 + 2b \cdot \varphi \cdot p_{sat} + c\right)} \tag{12}$$

3.3. Validation of moisture buffer behaviour on Wufi® Pro

The simulation results on WUFI® Pro were comprehensively analysed to evaluate the accuracy of the model in replicating the material behaviour under transient hygrothermal conditions. The analysis consisted of comparing the simulated results against measured data across a range of surface resistances.

Fig. 5 highlights the significant influence of surface resistance on the accuracy of the simulation results. As demonstrated in the bar charts: plot (a) displays the percentage errors between the measured and simulated mass variations for the two samples across different values of surface resistances.

The lowest errors for both Δm and MBV were generally observed at a surface resistance of 0.1 m^2K/W, with values of 0.67 % for lime plaster and 1.59 % for alginate plaster. This confirms that 0.1 m^2K/W offers the best overall agreement between measured and simulated values. Plot (b) mirrors the first one in its structure, presenting percentage errors between measured and simulated MBV values, derived from the moisture content simulated data under different surface resistances. However, for the lime plaster, MBV prediction was more accurate at 0.13 m^2K/W, indicating a potential material-specific sensitivity to boundary conditions. This variability highlights the importance of carefully calibrating surface resistances based on the material's hygrothermal properties, to ensure robust and accurate simulation outcomes.

Fig. 6 further investigates the performance of the model for the alginate plaster using a surface resistance of 0.1 m^2K/W. This analysis is crucial for assessing the model's ability to accurately predict changes in moisture buffer behaviour within the material under test conditions. Specifically, subplot (a) reveals a strong correlation between the experimental and simulated mass changes, confirming the model's capability to capture dynamic moisture interactions. Subplots (b) provides an additional examination of the mass changes by plotting measured vs. simulated mass variations for cycles 2 to 7 (Fig. 6). The dispersion of data points relative to the graph bisector reflects the simulation's precision with different cycles of the testing protocol. In particular, the tight clustering of data points around the bisector indicates a high level of accuracy across repeated sorption–desorption cycles.

The comprehensive hygrothermal characterization of samples was crucial for deriving diffusivity and the water vapour diffusion resistance factor and establishing a fundamental dataset for accurate simulations. In addition, these results highlight the relevance of the assumption of the surface resistance coefficient to improve simulation accuracy across different plasters. This rigorous validation of two materials, further detailed in section A4 of the Supplementary, confirms the validity of this approach. This result has enabled the implementation of the estimated materials properties in a room-scale simulation model on WUFI® Plus, facilitating future assessments of their impact on indoor humidity stabilization and energy performance at the room level.

3.4. Modelling plaster influence at the room scale with WUFI® plus

This section presents the results of room-scale simulations evaluating the influence of plaster type on indoor φ. The performance of alginate and lime plasters is compared under two temperature control scenarios (as summarized in Table 5). Temperature control in selections of Case 1.x kept indoor temperature between 20 °C and 26 °C during the working hours (8-18) and between 15 °C and 30 °C

Table 6
Interpolating coefficients for the vapour resistance factor of the lime and alginate plasters based on Eq. (10), as a function of the vapour pressure.

	a	b	c
Lime plaster	$1.4351 \cdot 10^{-9}$	$-5.5729 \cdot 10^{-6}$	$8.8420 \cdot 10^{-3}$
Alginate plaster	$1.9634 \cdot 10^{-8}$	$-5.1396 \cdot 10^{-5}$	$8.9313 \cdot 10^{-2}$

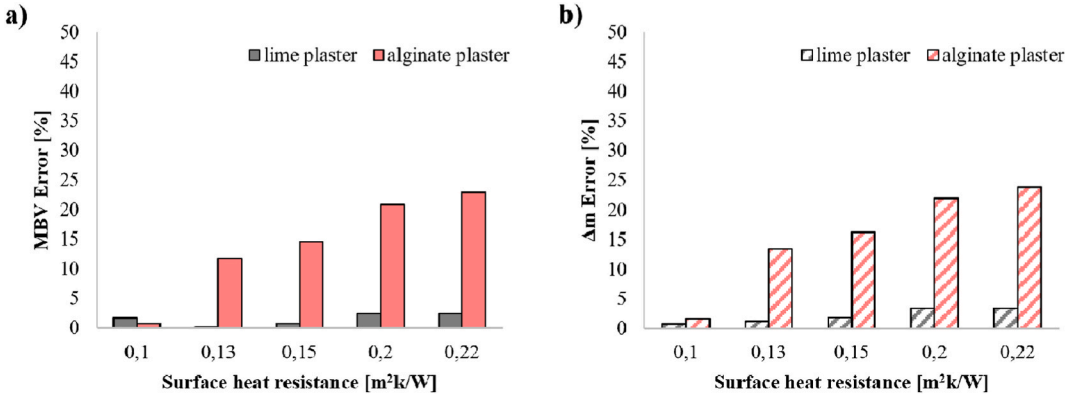

Fig. 5. Bar graph of percentage errors between measured values and simulated ones for different surface resistances and for the two samples: a) Mass Variation Analysis (Δm) b) MBV Analysis.

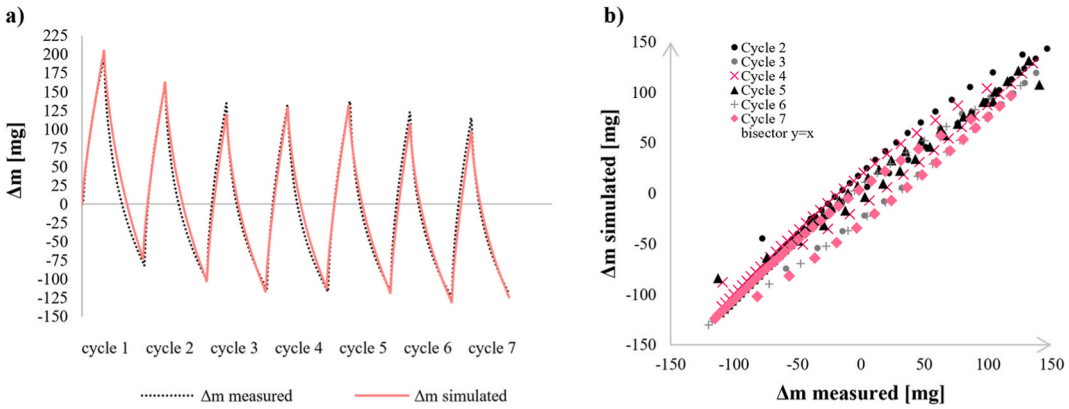

Fig. 6. a) Comparison of measured and simulated mass variations for the alginate plaster with a surface resistance of 0.1 m^2K/W b) Measured vs. simulated graph for mass variation of alginate plaster sample excluding the first cycle of the testing protocol, with a surface resistance of 0.1 m^2K/W.

during the rest of the day (18-8) without seasonal differences. On the contrary, temperature control in selections of Case 2.x followed a seasonal strategy. During heating season (from 01/01 to 15/04 and from 15/10 to 31/12) temperature is set at 20 °C during working hours (8-18), fluctuating between 15 and 30 °C during the rest of the day (18-8). While during the cooling season (from 01/01 to 15/04 and from 15/10 to 31/12) the temperature is set at 26 °C during working hours (8-18), fluctuating between 15 and 30 °C during the rest of the day (18-8). In each of the scenarios of temperature control, humidity was managed in free-running conditions (Case x.1), and with active humidity control (Cases x.2 and x.3). The aim is to quantify the enhanced capability of alginate plaster to passively regulate φ and to assess its impact on energy demand, particularly for cooling and dehumidification. Two types of analyses were carried out: i) the attenuation of indoor humidity fluctuations provided by alginate plaster compared with the reference lime plaster, and ii) the evaluation of dehumidification loads and the associated cooling energy consumption in both cases.

3.4.1. Attenuation of indoor humidity fluctuations

The overall effects in indoor φ fluctuations with the alginate plasters are shown in Fig. 7, where yearly trend of indoor φ are depicted for both plaster configuration against the outdoor φ, for the Case 2.1, in which the temperature is controlled during the working hours and kept steady at 20 °C during the heating period and at 26 °C for the rest of the year, with no active control on φ. In Fig. 7a the ability of the alginate plaster to buffer humidity oscillations is qualitatively evident. Indeed, indoor φ varies from 30 % to 70 % with alginate plaster, while it fluctuates between 28 % and 90 % with lime plaster. Fig. 7b shows that the maximum indoor φ obtained with the alginate plaster is generally lower than with lime plaster, whereas Fig. 7c indicates that the minimum φ over the year is consistently higher with alginate.

These results indicate a clear smoothing of the annual indoor humidity profile, with φ values more frequently confined within the desirable 40–60 % range (appropriate for acceptable indoor air quality in buildings). This effect is clearly illustrated in Fig. 8, which reports the cumulative frequency of φ values for the cases without active humidity control by the HVAC system (Cases 1.1 and 2.1). The alginate curves exhibit an S-shape distribution that is more compact compared to lime plaster, cutting out 30 % of yearly hours where φ is lower than 40 % and higher than 60 %. However, because the cumulative sorting procedure removes seasonal distinctions for the same φ values, the graph does not reveal pronounced differences between the two cases, even though seasonal variations in

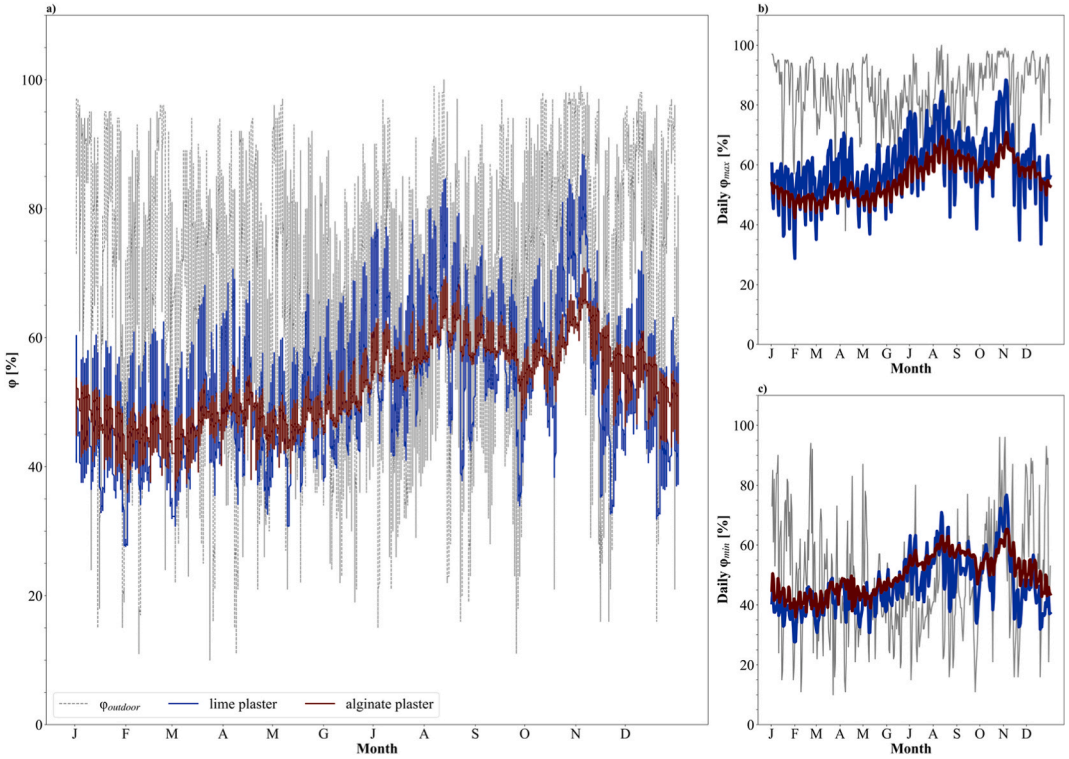

Fig. 7. Analysis of the effects of alginate plaster on humidity control. a) annual trend of indoor relative humidity considering the two plasters (Case 2.1); b) annual trend of maximum φ (Case 2.1) and minimum φ (Case 2.1) (c) indoor relative humidity.

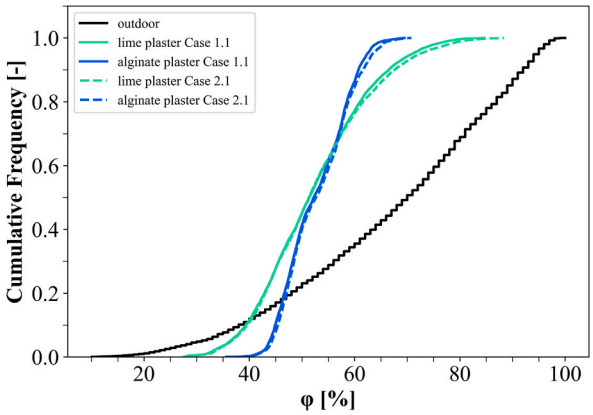

Fig. 8. Cumulative frequency functions of the relative humidity inside the simulated room with and without alginates, compared to the external air for the scenario Case 1.1 (φ uncontrolled, T controlled with constant setpoint) and Case 2.1 (φ uncontrolled, and T controlled with seasonal variation of set point).

temperature control are occurring.

To emphasize seasonal differences among the simulated cases, the monthly average of the attenuation factor f_φ was calculated and reported in Fig. 9, where the shaded bands indicate the monthly average deviation from the mean value. All simulated cases yielded positive f_φ values throughout the year, confirming the consistent damping effect of the alginate plaster compared to the lime plaster. No negative values were recorded, in accordance with the expected hygroscopic behaviour of the alginate plaster. In addition, the higher the f_φ, the more capable is the alginate plaster to mitigate the oscillations of φ compared to the lime plaster.

Fig. 9a highlights the main similarities and differences for the cases without active humidity control (Cases x.1). In particular, the alginate plaster showed the strongest buffering effect, with higher f_φ values in both cases, while some differences are particularly evident during the transitional periods of March–April and September–November. Likely, this is because the constant indoor

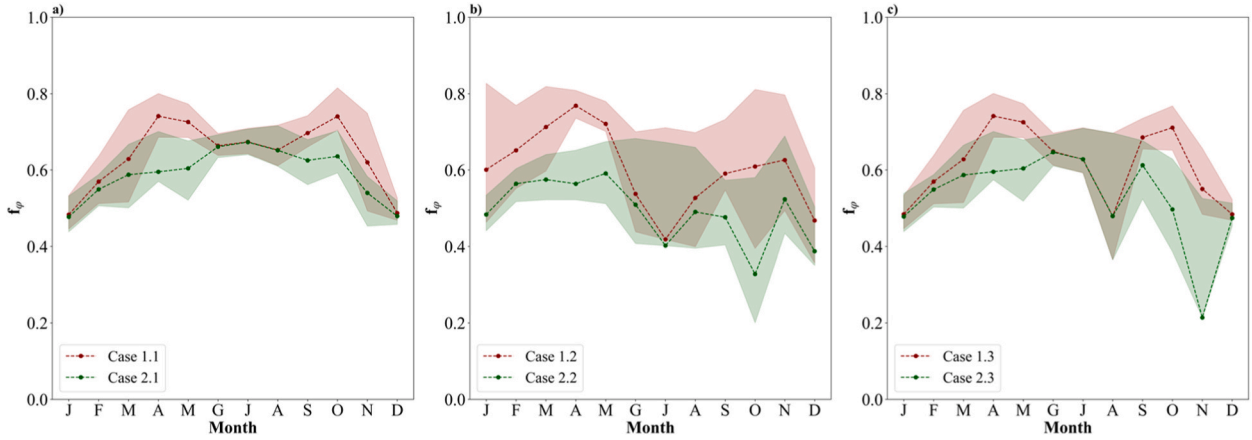

Fig. 9. Annual trend of attenuation factor f_φ in the six simulated cases.

temperature setpoint reduces temperature-driven φ swings, allowing the plaster's contribution to stand out. When φ control is active (Cases 1.2, 1.3, 2.2, 2.3), the HVAC system already limits φ variations, so the plaster has a lower impact. However, comparable deviations are also observed in the other cases in the same March–April and September–November periods.

In general, subcases x.2 and x.3 have lower f_φ values, especially in the warmer months when dehumidification is more intensive. Furthermore, the width of the shaded area (which reflects the magnitude of fluctuations in the moisture buffering effect) increases as the level of active φ control becomes more restrictive (progressively from Fig. 9b to c to Fig. 9a, corresponding to φ control ranges of 40–60 %, 30–70 %, and no control, respectively).

These results confirm what is commonly found also in other works [70–72], that the hygric behaviour of the high MBV materials is strongly influenced by the indoor environmental control strategy, and its presence can be used to relax set points of the HVAC control strategy. To further assess their impact, the following section evaluates how these materials affect dehumidification loads and related energy consumption.

3.4.2. Dehumidification loads and cooling energy consumption

The subsequent analysis quantified the benefits offered by the application of alginate plaster in reducing the energy consumption for both dehumidification and cooling. This evaluation refers to all simulated cases.

Fig. 10 illustrates the annual cooling demand for each case, divided into sensible and latent components. As visible in the chart, the sensible cooling demand remains substantially similar between lime and alginate plaster configuration within the same case. However, in some cases the demand is even slightly higher for the alginate plaster, likely due to its higher thermal conductivity (0.632 W/mK vs. 0.408 W/mK for lime plaster), corresponding to a 55 % higher thermal conductivity for the alginate plaster compared to the lime plaster, as reported in Table 3. On the other hand, the latent cooling demand is consistently and significantly reduced when alginate plaster is applied, particularly in Cases 1.2, 1.3, 2.2, and 2.3. In Cases 1.3 and 2.3, the latent cooling demand for the alginate plaster case drops to nearly zero, while lime plaster still requires 15 kWh and 19 kWh, respectively. This behaviour is primarily explained by the wider indoor humidity control band adopted in these scenarios (30–70 % φ during working hours), within which the alginate plaster maintains indoor φ without triggering the dehumidification coil. A detailed hourly analysis for August—the month exhibiting the highest dehumidification demand—supporting this finding is provided in the Supplementary Information (Section A5). This is also clearly demonstrated in Table 7, where the latent cooling demand reduction compared to lime plaster reaches 100 % in Case 1.3 and 99.60 % in Case 2.3. In Cases 1.2 and 2.2, where stricter indoor humidity control was imposed in the simulations (φ set between 40 % and 60 %), the reductions in latent cooling demand are still significant, though not total, amounting to 63.51 % and 57.46 %, respectively, compared to lime plaster (Table 7). As a result, the total cooling demand (sensible + latent) is generally lower when alginate plaster is used, with maximum reductions up to 11.17 % (Case 1.2). However, this is not observed in Cases 1.1, 2.1, and 2.3, where the total cooling demand is similar or slightly higher for alginate plaster. In Cases 1.1 and 2.1, this is attributable to the absence of latent demands (due to no φ control), which makes the sensible demand—and thus the thermal properties of the plaster—the dominant factor. In Case 2.3, although the latent component is nearly zero, the total demand slightly increases (574 kWh for alginate plaster vs. 568 kWh for lime plaster), with a negligible percentage difference of only 0.94 %, again due to the higher thermal conductivity of the alginate plaster. These values are comparable with ones obtained by [73] with similar exposed surfaces, but with a material with a MBV of 1 g/m^2 %.

Overall, the total cooling demand is generally lower in Cases 1.1, 1.2, and 1.3 compared to the corresponding Cases 2.1, 2.2, and 2.3, which can be attributed to the less stringent temperature control strategy applied in the former. In Cases 1.x, the indoor temperature is maintained between 20 °C and 26 °C during working hours and allowed to fluctuate between 15 °C and 30 °C during the rest of the day throughout the year. In contrast, in Cases 2.x, the indoor temperature is strictly set at 26 °C during the entire non-heating season (from mid-April to mid-October) during working hours, with the same fluctuation range (15–30 °C) applied during non-working hours. This tighter temperature regulation in Cases 2.x contributes to higher sensible cooling demands overall.

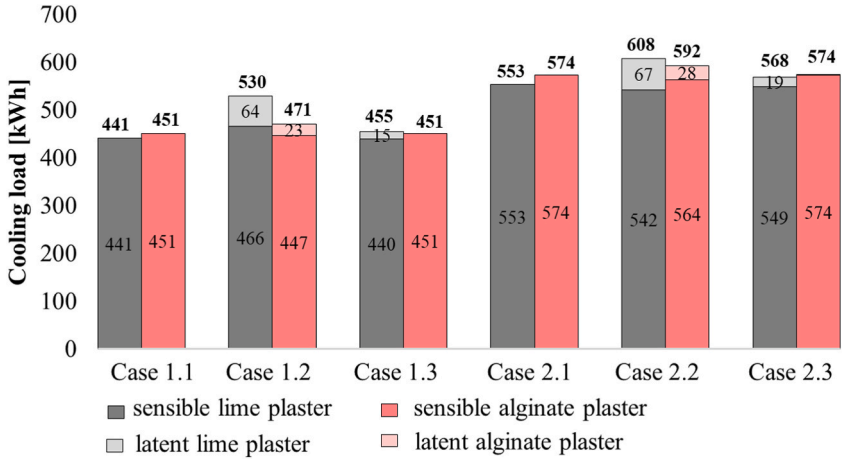

Fig. 10. Annual cooling demand (kWh), including sensible and latent components, for lime and alginate plasters across all cases.

Table 7
Annual comparison of dehumidification demand and energy consumption for different plasters.

	Case 1.2		*Case 1.3*		*Case 2.2*		*Case 2.3*	
	Lime plaster	*Alginate plaster*	*Lime plaster*	*Alginate plaster*	*Lime plaster*	*Alginate plaster*	*Lime plaster*	*Alginate plaster*
Total latent cooling demand								
[kg]	102.31	37.33	24.74	0.00	106.88	45.47	31.15	0.12
[kWh]	63.95	23.33	15.46	0.00	66.80	28.42	19.47	0.08
Reduction of latent cooling demand with alginate [%]	**−63.51 %**		**−100 %**		**−57.46 %**		**−99.60 %**	
Total cooling demand (sensible and latent) [kWh]	529.87	470.66	455.02	451.09	608.48	591.96	568.31	573.63
Reduction of total cooling demand with alginate [%]	**−11.17 %**		**−0.86 %**		**−2.71 %**		**+0.94 %**	
Latent cooling fraction of total cooling demand [%]	**12.07**	**4.96**	**3.40**	**0.00**	**10.98**	**4.80**	**3.43**	**0.01**

These results confirm that the use of alginate plaster can lead to substantial energy savings in building cooling, particularly when humidity control is present and latent demands are significant, mainly thanks to its hygroscopic buffering capacity.

Table 7 reports the annual comparison of latent cooling demand and total cooling demand for lime plaster and alginate plaster in selected cases. Cases 1.1 and 2.2 were excluded, as no relative humidity control was applied in the simulations, resulting in no dehumidification demand. The table includes latent cooling expressed in terms of dehumidification demands [kg] and the related energy consumption [kWh], percentage reductions for dehumidification compared to lime plaster, total cooling demand (sensible + latent), and the share of latent cooling over the total demand.

Moreover, Table 7 complements the previous analysis by providing a detailed quantitative comparison of latent cooling demands and related energy consumption.

The reduction in latent cooling demand when using alginate plaster is particularly evident in Cases 1.3 and 2.3, where values drop to nearly zero (0.00 and 0.12 kg respectively), leading to an almost complete suppression of latent cooling demand. This behaviour is analysed and contextualised in the Supplementary Information (section A5), where hourly profiles of the cooling loads for the month of August are reported.

Among all cases, Case 1.2 shows the most significant overall energy savings, with a reduction in latent energy consumption of 63.51 % and a decrease in total cooling demand of 11.17 %. This is also reflected in the latent share, which drops from 12.07 % to 4.96 %. On the other hand, in Case 2.3, the excellent latent demand reduction is offset by a slight increase in the sensible component, leading to a marginal increase in total cooling demand (+0.94 %).

These findings highlight the promising role that alginate plaster plays for stabilizing indoor humidity levels and significantly reducing energy expenses related to air control. Its application suggests substantial potential for innovative passive strategies in new constructions and retrofitting existing buildings.

The advantages of utilizing highly hygroscopic materials as internal finishing extend also to the improvement of comfort conditions. The reduction of the amplitude of air relative humidity oscillations due to moisture loads as shown in Figs. 7 and 8, potentially improves the comfort levels of the occupants. This effect could be more relevant in cases without HVAC systems and higher air temperatures, when high moisture loads are the main driver of occupants' discomfort. In these cases, materials with high MBV could

help improve significantly comfort, but a realistic evaluation of the phenomenon would require an extensive hygroscopic characterization of the materials and extended heat and moisture transfer models, that could consider temperature-variable moisture adsorption isotherms. Future work on this topic is therefore required to establish the effective performance of highly hygroscopic materials as internal finishing.

4. Conclusions

In this work, a new method for a simplified hygroscopic material characterization is proposed and it has been applied on two materials, an alginate enhanced plaster and a lime plaster, used as baseline. The material properties are used to evaluate the performance of the highly hygroscopic material used as internal finishing. The main findings of this work are hereby outlined:

- Using a Fickian diffusion model fitted to RH step-response data from a dynamic vapour sorption (DVS) analyzer (model interpolated through minimizing the root-mean-square error) we estimated the effective moisture diffusivity as $D \sim 1.84 \times 10^{-8}$ m^2s^{-1} for the lime plaster and $D \sim 1.17 \times 10^{-9}$ $m^2s^{-1}$for the plaster containing 20 % calcium alginate. Over the investigated range, the dependence of D on moisture content was negligible.
- Vapour resistance factor functions—derived from the fitted diffusivities and the materials' sorption isotherms—were used to validate the models against MBV dynamic tests following the NORDTEST protocol. The best agreement for both mass change (Δm) and MBV was obtained with a surface resistance of 0.1 m^2KW^{-1}, yielding percentage errors of 0.67 % for the lime plaster and 1.59 % for the alginate plaster. The overlay of measured and simulated Δm trends demonstrated the model's capability to reproduce the dynamic hygric response of the materials across repeated sorption–desorption cycles.
- 5 years simulations at room scale have demonstrated that the enhanced alginate plaster has buffered indoor φ fluctuations more effectively than lime plaster, with attenuation factors (f_φ) ranging between ~0.2 (strictly controlled, winter period) and ~0.8 (uncontrolled, spring period) depending on boundary conditions;
- Energy consumption analysis highlighted substantial reductions in latent cooling demand: 63.5 % in Case 1.2, ~100 % in Cases 1.3 and 2.3 (wider indoor relative humidity control band), and 99.6 % in Case 2.2 compared to lime plaster. Total cooling energy demand decreased by up to 11.2 % in Case 1.2 when alginate plaster was applied, while sensible cooling demand remained similar between plasters.

These results demonstrate the dual benefit of enhanced alginate plaster in stabilizing indoor humidity and reducing cooling energy use, confirming its potential as a passive strategy for energy-efficient building design and retrofitting applications.

CRediT authorship contribution statement

V. Gentile: Writing – review & editing, Writing – original draft, Visualization, Validation, Supervision, Software, Project administration, Methodology, Investigation, Formal analysis, Data curation, Conceptualization. **G. Autretto:** Writing – review & editing, Writing – original draft, Visualization, Validation, Software, Methodology, Investigation, Formal analysis, Data curation, Conceptualization. **M. Libralato:** Writing – review & editing, Methodology, Data curation, Conceptualization. **S. Fantucci:** Writing – review & editing, Supervision, Project administration, Methodology, Investigation, Funding acquisition, Conceptualization. **V. Serra:** Writing – review & editing, Supervision, Project administration, Methodology, Funding acquisition, Conceptualization.

Declaration of competing interest

We confirm that the manuscript has been read and approved by all named authors and that there are no other persons who satisfied the criteria for authorship but are not listed. We further confirm that all have approved the order of authors listed in the manuscript.

We confirm that we have given due consideration to the protection of intellectual property associated with this work and that there are no impediments to publication, including the timing of publication, concerning intellectual property. In so doing, we confirm that we have followed the regulations of our institutions concerning intellectual property.

The authors Vincenzo Gentile, Valentina Serra, Stefano Fantucci and Giorgia Autretto reports financial support for the methodology validation thanks to the Project “Choisis- Characterisation of Innovative and Sustainable Insulating Solutions”, funded within the Italian National Recovery and Resilience Plan (PNRR), Mission 4 – Education and Research- Measure M4C2 – Investment 1.1 PRIN – Research programs of national interest – project code 2022372TM9, CUP F53D23001540006. While the room scale simulation was carried out within the Activity 18 -PTR_19_21_ENEA_PRG_4 2019–2022 funded by Italian Ministry of Economic Development (MiSE) and the Italian National Agency for New Technologies, Energy and Sustainable Economic Development (ENEA).

We understand that the Corresponding Author is the sole contact for the Editorial process (including the Editorial Manager and direct communications with the office). He is responsible for communicating with the other authors about progress, submissions of revisions, and final approval of proofs.

We confirm that we have provided a current, correct email address which is accessible by the Corresponding Author and which has been configured to accept email from *vincenzo.gentile@polito*.it.

Acknowledgements

The methodology validation was possible thanks to the Project "Choisis- Characterisation of Innovative and Sustainable Insulating Solutions", funded within the Italian National Recovery and Resilience Plan (PNRR), Mission 4 – Education and Research- Measure M4C2 – Investment 1.1 PRIN – Research programs of national interest – project code 2022372TM9, CUP F53D23001540006. The room scale simulation was carried out within the Activity 18 -PTR_19_21_ENEA_PRG_4 2019–2022 funded by Italian Ministry of Economic Development (MiSE) and the Italian National Agency for New Technologies, Energy and Sustainable Economic Development (ENEA).

Appendix A. Supplementary data

Supplementary data to this article can be found online at https://doi.org/10.1016/j.jobe.2025.114983.

Data availability

Data will be made available on request.

References

[1] M. Woloszyn, T. Kalamees, M.O. Abadie, M. Steeman, A. Sasic Kalagasidis, The effect of combining a relative-humidity-sensitive ventilation system with the moisture-buffering capacity of materials on indoor climate and energy efficiency of buildings, Build. Environ. 44 (2009) 515–524.
[2] S. Liuzzi, M.R. Hall, P. Stefanizzi, S.P. Casey, Hygrothermal behaviour and relative humidity buffering of unfired and hydrated lime-stabilised clay composites in a mediterranean climate, Build. Environ. 61 (2013) 82–92.
[3] H. Yoshino, T. Mitamura, K. Hasegawa, Moisture buffering and effect of ventilation rate and volume rate of hygrothermal materials in a single room under steady state exterior conditions, Build. Environ. 44 (2009) 1418–1425.
[4] M. Qin, P. Hou, Z. Wu, J. Wang, Precise humidity control materials for autonomous regulation of indoor moisture, Build. Environ. 169 (2020) 106581.
[5] J. Woods, J. Winkler, Effective moisture penetration depth model for residential buildings: sensitivity analysis and guidance on model inputs, Energy Build. 165 (2018) 216–232.
[6] Z. Yang, W. Zhang, X. Lin, Q. Xiong, Q. Jiang, Optimization of minor-licl-modified gypsum as an effective indoor moisture buffering material for sensitive and long-term humidity control, Build. Environ. 229 (2023) 109962.
[7] D. Smyl, F. Ghasemzadeh, M. Pour-Ghaz, Modeling water absorption in concrete and mortar with distributed damage, Constr. Build. Mater. 125 (2016) 438–449.
[8] P. Brimblecombe, B. Ramer, Museum display cases and the exchange of water vapour, Stud. Conserv. 28 (4) (1983) 179–188, https://doi.org/10.1179/sic.1983.28.4.179.
[9] D. Camuffo, G. Sturaro, A. Valentino, Showcases: a really effective mean for protecting artworks? Thermochim. Acta 365 (2000) 65–77.
[10] Garry Thomson, Stabilization of RH in exhibition cases: hygrometric half-time, Stud. Conserv. 22 (1977) 85–102.
[11] G.B.A. Coelho, H.E. Silva, F.M.A. Henriques, Calibrated hygrothermal simulation models for historical buildings, Build. Environ. 142 (2018) 439–450.
[12] Florence Collet, Stijn Mertens, Paulina Faria, Sofiane Amziane, Thibaut Colinart, Camille Magniont, R.D.T.F. Sylvie Prétot, M.L. Rilem, TC 275 HDB – international RRT on MBV Measurement of Vegetal Concrete, in: International RILEM Conference on Synergising Expertise Towards Sustainability and Robustness of Cement-based Materials and Concrete Structures, 2023, pp. 1279–1287, 1.
[13] D. Lelièvre, T. Colinart, P. Glouannec, Modeling the moisture buffering behavior of a coated biobased building material by including hysteresis, Energy Proc. 78 (2015) 255–260.
[14] M. Posani, et al., Low-carbon indoor humidity regulation via 3D-printed superhygroscopic building components, Nat. Commun. 16 (2025).
[15] Y. Aït Oumeziane, S. Moissette, M. Bart, F. Collet, S. Pretot, C. Lanos, Influence of hysteresis on the transient hygrothermal response of a hemp concrete wall, J. Build. Perform. Simul. 10 (3) (2017) 256–271, https://doi.org/10.1080/19401493.2016.1216166.
[16] R. Bui, J. Goffart, F. McGregor, A. Fabbri, M. Woloszyn, A.C. Grillet, Hygrothermal behaviour of a rammed earth wall subjected to realistic conditions: investigation of the most influential parameters, J. Build. Perform. Simul. (2025) 1–18, https://doi.org/10.1080/19401493.2025.2525421.
[17] Tran Le, C. Maalouf, O. Douzane, G. Promis, T.H. Mai, T. Langlet, Impact of combined moisture buffering capacity of a hemp concrete building envelope and interior objects on the hygrothermal performance in a room, J. Build. Perform. Simul. 9 (6) (2016) 589–605, https://doi.org/10.1080/19401493.2016.1160434.
[18] S. El Hassani, M. Charai, M.A. Moussaoui, A. Mezrhab, Towards rural net-zero energy buildings through integration of photovoltaic systems within bio-based earth houses: case study in Eastern Morocco, Sol. Energy 259 (2023) 15–29.
[19] D. Ding, M. Qin, Comparative study of Metal-Organic frameworks (MOFs) for indoor moisture control, Appl. Therm. Eng. 257 (2024) 124329.
[20] L. Senff, et al., Development of mortars containing superabsorbent polymer, Constr. Build. Mater. 95 (2015) 575–584.
[21] S. Liuzzi, M.R. Hall, P. Stefanizzi, S.P. Casey, Hygrothermal behaviour and relative humidity buffering of unfired and hydrated lime-stabilised clay composites in a Mediterranean climate, Build. Environ. 61 (2013) 82–92.
[22] B. Mazhoud, F. Collet, S. Pretot, J. Chamoin, Hygric and thermal properties of hemp-lime plasters, Build. Environ. 96 (2016) 206–216.
[23] S. Cerolini, M. D'Orazio, C. Di Perna, A. Stazi, Moisture buffering capacity of highly absorbing materials, Energy Build. 41 (2009) 164–168.
[24] V. Cascione, D. Maskell, A. Shea, P. Walker, M. Mani, Comparison of moisture buffering properties of plasters in full scale simulations and laboratory testing, Constr. Build. Mater. 252 (2020) 119033.
[25] V. Gentile, M. Libralato, S. Fantucci, L. Shtrepi, G. Autretto, Enhancement of the hygroscopic and acoustic properties of indoor plasters with a super adsorbent calcium alginate BioPolymer, J. Build. Eng. 76 (2023) 107147, https://doi.org/10.1016/j.jobe.2023.107147.
[26] H. Garbalińska, M. Bochenek, W. Malorny, J. von Werder, Comparative analysis of the dynamic vapor sorption (DVS) technique and the traditional method for sorption isotherms determination — exemplified at autoclaved aerated concrete samples of four density classes, Cem Concr Res 91 (2017) 97–105.
[27] Carsten Rode, Ruut Hannele Peuhkuri, Lone Hedegaard Mortensen, Kurt Kielsgaard Hansen, Berit Time, Arild Gustavsen, Tuomo Ojanen, Jarkko Ahonen, Kaisa Svennberg, Jesper Arfvidsson. Moisture Buffering of Building Materials, BYG Report No R-127, Technical University of Denmark, Department of Civil Engineering, 2005.
[28] V. Cascione, D. Maskell, A. Shea, P. Walker, M. Mani, Comparison of moisture buffering properties of plasters in full scale simulations and laboratory testing, Constr. Build. Mater. 252 (2020) 119033.
[29] V. Cascione, D. Maskell, A. Shea, P. Walker, A review of moisture buffering capacity: from laboratory testing to full-scale measurement, Constr. Build. Mater. 200 (2019) 333–343.
[30] M. Zhang, M. Qin, C. Rode, Z. Chen, Moisture buffering phenomenon and its impact on building energy consumption, Appl. Therm. Eng. 124 (2017) 337–345.

[31] M. Yang, F. Kong, X. He, Moisture buffering effect of hygroscopic materials under wall moisture transfer, Indoor Built Environ. 31 (2022) 80–95.
[32] K. Zu, M. Qin, C. Rode, M. Libralato, Development of a moisture buffer value model (MBM) for indoor moisture prediction, Appl. Therm. Eng. 171 (2020) 115096.
[33] A. Ranesi, M. Posani, R. Veiga, P. Faria, A Discussion on Winter Indoor Hygrothermal Conditions and Hygroscopic Behaviour of Plasters in Southern Europe, Infrastructures 7 (2022) 38, https://doi.org/10.3390/infrastructures7030038.
[34] P. Magda, V. Vera, O. Pietro, E. Damaris, H. Guillaume, High-tech, low-carbon material fabrication: 3d-printed geopolymers for indoor hygrometric comfort improvement, in: CEES 2023 | 2nd International Conference on Construction, Energy, Environment & Sustainability, 2023.
[35] Y. Goto, et al., Heat and moisture balance simulation of a building with vapor-open envelope system for subtropical regions, Build. Simulat. 5 (2012) 301–314.
[36] D. Kaczorek, Moisture Buffering of Multilayer Internal Wall Assemblies at the Micro Scale: Experimental Study and Numerical Modelling, Appl. Sci. 9 (2019) 3438, https://doi.org/10.3390/app9163438.
[37] M. Barclay, N. Holcroft, A.D. Shea, Methods to determine whole building hygrothermal performance of hemp-lime buildings, Build. Environ. 80 (2014) 204–212.
[38] S. Cerolini, M. D'Orazio, C. Di Perna, A. Stazi, Moisture buffering capacity of highly absorbing materials, Energy Build. 41 (2009) 164–168.
[39] F. Mnasri, S. Bahria, M.E.A. Slimani, O. Lahoucine, M. El Ganaoui, Building incorporated bio-based materials: experimental and numerical study, J. Build. Eng. 28 (2020) 101088.
[40] M.O. Abadie, K.C. Mendonça, Moisture performance of building materials: from material characterization to building simulation using the moisture Buffer Value concept, Build. Environ. 44 (2009) 388–401.
[41] H. Wan, Z. Sun, G. Huang, X. Xu, J. Yu, Calculation of the maximum moisture buffering thickness of building wall layer of hygroscopic material, Build. Environ. 160 (2019) 106173.
[42] N. Reuge, et al., Modeling of hygrothermal transfers through a bio-based multilayered wall tested in a bi-climatic room, J. Build. Eng. 32 (2020) 101470.
[43] ISO 12570:2000+A2:2018, Hygrothermal Performance of Building Materials and Products - Determination of Moisture Content by Drying at Elevated Temperature, 2018.
[44] ASTM C1498-04a, Standard Test Method for Hygroscopic Sorption Isotherms of Building Materials, i, ASTM International, 2016, p. 4.
[45] ISO 12571:2021, Hygrothermal Performance of Building Materials and Products — Determination of Hygroscopic Sorption Properties, 2021, pp. 1–22.
[46] ISO 12572:2001, Hygrothermal Performance of Building Materials and Products —, 2001, p. 36.
[47] ASTM E3054/E3054M-16, Standard Guide for Characterization and Use of Hygrothermal Models for Moisture Control Design in Building Envelopes, vol. 8, 2016, https://doi.org/10.1520/E3054.
[48] ISO 12570:2000, Hygrothermal Performance of Building Materials and Products — Determination of Moisture Content by Drying at Elevated Temperature, International Organization for Standardization, Geneva, Switzerland, 2000.
[49] A.D. Tran Le, J.S. Zhang, Z. Liu, D. Samri, T. Langlet, Modeling the similarity and the potential of toluene and moisture buffering capacities of hemp concrete on IAQ and thermal comfort, Build. Environ. 188 (2021) 107455.
[50] T. Colinart, D. Lelievre, P. Glouannec, Experimental and numerical analysis of the transient hygrothermal behavior of multilayered hemp concrete wall, Energy Build. 112 (2016) 1–11.
[51] R. Ramirez, B. Ghiassi, P. Pineda, P.B. Lourenço, Simulation of moisture transport in fired-clay brick masonry structures accounting for interfacial phenomena, Build. Environ. 228 (2023) 109838.
[52] Z. Liu, Z. Dong, T. Zhou, L. Cao, Water vapor diffusion models in asphalt mortar considering adsorption and capillary condensation, Constr. Build. Mater. 308 (2021) 125049.
[53] B. Mazhoud, F. Collet, S. Pretot, J. Chamoin, Hygric and thermal properties of hemp-lime plasters, Build. Environ. 96 (2016) 206–216.
[54] H. Garbalińska, S.J. Kowalski, M. Staszak, Moisture diffusivity in mortars of different water-cement ratios and in narrow ranges of air humidity changes, Int. J. Heat Mass Tran. 56 (2013) 212–222.
[55] L. Pel, K. Hazrati, K. Kopinga, J. Marchand, Water absorption in mortar determined by NMR, Magn. Reson. Imaging 16 (1998) 525–528.
[56] V. Gentile, M. Calò, M. Bozlar, M. Simonetti, F. Meggers, Water vapor mass transfer in alginate–graphite bio-based hydrogel for atmospheric water harvesting, Int. J. Heat Mass Tran. 219 (2024) 1–13.
[57] M. Qin, O.S. Rasmussen, J. Chen, L. Wadsö, Novel MOF-based autonomous humidity control materials for energy-efficient indoor moisture regulation, Build. Environ. 261 (2024).
[58] X. Feng, M. Qin, S. Cui, C. Rode, Metal-organic framework MIL-100(Fe) as a novel moisture buffer material for energy-efficient indoor humidity control, Build. Environ. 145 (2018) 234–242.
[59] H.E. Huerto-Cardenas, et al., Validation of dynamic hygrothermal simulation models for historical buildings: state of the art, research challenges and recommendations, Build. Environ. 180 (2020) 107081.
[60] M.J. Powell, A hybrid method for nonlinear equations. Numerical Methods for Nonlinear Algebraic Equations, 1970, pp. 87–161.
[61] J. Crank, The mathematics of diffusion, J. Am. Chem. Soc. (1975), https://doi.org/10.1021/ja01562a072. Clarendon press Oxford.
[62] M. Barclay, N. Holcroft, A.D. Shea, Methods to determine whole building hygrothermal performance of hemp-lime buildings, Build. Environ. 80 (2014) 204–212.
[63] iClimabuilt project, 2021, https://iclimabuilt.eu/, 2021.
[64] Manuela Baracani, G.L. Belviso, F. F, V. S, A. P, Influence of sensing infrastructure resolution and comfort models integration on the thermal comfort evaluation of an office space, in: U. Berardi (Ed.), Multiphysics and Multiscale Building Physics, Springer Nature Singapore, Singapore, 2025, pp. 233–238.
[65] ASHRAE, ASHRAE 55-2017 - Thermal Environmental Conditions for Human Occupancy, 2017.
[66] International Energy Agency (IEA), A. 41, IEA Annex 41 Whole Building Heat, Air, Moisture Response, 2008.
[67] EN 16798-1: Energy Performance of Buildings- Ventilation for Buildings Part 1: Indoor Environmental Input Parameters for Design and Assessment of Energy Performance of Buildings Addressing Indoor Air Quality, Thermal Environment, Lighting and Acoustics- Module M1-6, European Committee for Standardization, Brussels, 2019.
[68] M.K. Kumaran, Moisture diffusivity of building materials from water absorption measurements, J. Therm. Envelope Build. Sci. 22 (1999) 349–355.
[69] Hartwig Künzel. Simultaneous Heat and Moisture Transport in Building Components, One- and two-dimensional calculation using simple parameters, 1995. https://publica-rest.fraunhofer.de/server/api/core/bitstreams/74f34b4c-4876-4a9b-ac87-f7476d48ca60/content.
[70] D. Ding, O.S. Rasmussen, M. Qin, Moisture buffer value for hygroscopic materials with different thicknesses, Build. Environ. 258 (2024).
[71] Clemence Legros, Matthieu Cosnier, Monika Woloszyn, Amandine Piot 3, M. P. Impact of moisture buffering for improving summer comfort in buildings, Proceedings of Building Simulation 2019: 16Th Conference of IBPSA. (2019), https://doi.org/10.26868/25222708.2019.211054.
[72] M. Larcher, et al., Assessing the impact of moisture buffering properties of materials on indoor environmental quality: a study on a recycled material plaster, Build. Environ. 267 (2025) 112170.
[73] M. Winkler, K. Nore, F. Antretter, NSB (2014).